Electrochemical Signatures of Potassium Plating and Stripping

Electrochemical Signatures of Potassium Plating and Stripping

Journal of The Electrochemical Society, 2024 **171** 020517

Electrochemical Signatures of Potassium Plating and Stripping

Josef Rizell, Wojciech Chrobak, Nataliia Mozhzhukhina, Shizhao Xiong, and Aleksandar Matic[z]

Department of Physics, Chalmers University of Technology, SE–412 96 Göteborg, Sweden

Alkali metal anodes can enable unmatched energy densities in next generation batteries but suffer from insufficient coulombic efficiencies. To deduce details about processes taking place during galvanostatic cycling, voltage profiles are commonly analyzed, however the interpretation is not straightforward as multiple processes can occur simultaneously. Here we provide a route to disentangle and interpret features of the voltage profile in order to build a mechanistic understanding on alkali metal stripping and deposition, by investigating potassium metal deposition as a model case where processes and reactions are exaggerated due to the high reactivity of potassium. In particular, the importance of separating SEI formation and nucleation to correctly estimate the energy barrier for nucleation is demonstrated. Further, we show how the native layer formed on alkali metal foils gives rise to strong features in the voltage profile and propose forming alkali metal electrode through electrodeposition to mitigate these effects.
 [DOI: 10.1149/1945-7111/ad2593]

Manuscript submitted October 30, 2023; revised manuscript received December 28, 2023. Published February 13, 2024.

Supplementary material for this article is available online

Due to their high theoretical specific capacities and low reduction potentials, alkali metals are attractive anode materials for high energy density batteries.[1] Several concepts with metals anodes, including anode free cells, have been proposed in literature showing potential to significantly improve energy density in cells with both liquid and solid electrolytes.[2,3] However, the application of metal anodes and anode free concepts in practice is currently hindered by insufficient coulombic efficiencies,[4] associated to the uneven deposition and stripping,[1] and the side reactions between the deposited alkali metal and the electrolyte.[5] For instance, dendritic deposits lead to the formation of a porous morphology and growth of the solid electrolyte interphase (SEI) resulting in a continuous electrolyte consumption and depletion of active material.[5] Additionally, when uneven metal deposits are stripped from the electrode, part of the fragile dendritic structures often become disconnected from the bulk electrode and electronically insulated, forming so-called "dead" metal.[6] To develop efficient mitigation strategies to these problems, it is necessary to build a more detailed understanding of the processes occurring at the electrodes during plating and stripping, as well as of the methods used to study these phenomena.

During plating (charge) and stripping (discharge) on a metal anode, four separate processes can be distinguished: (1) Side reactions due to the low reduction potential of the alkali metal, which is outside the electrochemical window of most liquid electrolytes, and their high chemical reactivity. Part of these reactions will contribute to the formation of a passivating solid electrolyte interphase (SEI) film on the surface of the electrode.[7] (2) Nucleation as the first step of metal deposition on a substrate after reduction of alkali ions from the electrolyte forming clusters of metal atoms on the surface.[8,9] (3) Growth of the nuclei to a continuous metal phase as the deposition process proceeds.[10] (4) Stripping, during cell discharge, where the alkali metal will be oxidized leading to removal of alkali metal from the electrode surface.[11,12]

To investigate and understand these processes, galvanostatic experiments are often performed in idealized cells. Symmetric cells, where both electrodes are identical alkali metal electrodes, are typically used to evaluate the compatibility of an electrolyte to the anode material through the stability of the overpotential.[12–15] In asymmetric cells, where the working electrode is an inert substrate, often copper, and the counter electrode is an alkali metal foil, the coulombic efficiency can also be determined.[16,17] Further, this type of cell is the archetype in anode free configurations.[2] To deduce details about the central processes taking place during plating and stripping on the working electrode, the voltage profile is analyzed. For instance, the growth of large dendritic structures short-circuiting the cell is marked by a sharp decrease in (over)voltage.[18] Continuous SEI buildup over repeated cycling is instead manifested as a gradually increasing overvoltage.[19] At the start of deposition, the nucleation process is generally identified by an overvoltage peak, frequently used to analyze the energy barrier for nucleation.[20] However, several different processes often occur simultaneously, making them difficult to disentangle and erroneous conclusions can easily be drawn from a simple inspection of the voltage profile.

Here we demonstrate a route to obtain direct insight in the separate processes during plating and stripping which is necessary to build a mechanistic understanding around alkali metal anodes. The aim is to disentangle the contributions of side reactions, nucleation, growth and stripping to the voltage profiles during galvanostatic cycling. We use three-electrode measurements and electrochemical techniques, such as cyclic voltammetry, chronoamperometry and chronopotentiometry, in asymmetric K–Cu cells to separate the different processes. Most of the research on alkali metal anodes has been focused on lithium, which is the metal anode with the highest theoretical specific capacity. However, the heavier but more abundant metals sodium and potassium also have great potential as electrode materials.[21,22] Here, we study potassium metal anodes to learn more about aspects of alkali metal stripping and their electrochemical signatures. Potassium shares many similarities with lithium and sodium, but in many cases the phenomena are exaggerated and processes more pronounced, due to a higher reactivity of potassium metal[23] and the formation of a different SEI.[22]

Experimental

Preparation of materials.—The electrolyte was prepared by mixing potassium bis(fluorosulfonyl)imide (KFSI) (Solvionic) and 1,2-dimethoxyethane (DME) (Sigma Aldrich) in a 1:2.5 molar ratio. To ensure complete dissolution of the salt, the solution was magnetically stirred for at least 24 h at room temperature.

K metal foil was prepared from K metal chunks (Apollo Scientific, 97% and Sigma Aldrich, 98%). All edges of the chunk were removed using a scalpel, creating a cube with fresh K surfaces which was sandwiched between two sheets of Celgard (2400) separator and rolled to a 200 μm thick foil using a hand-operated roller (WCHO-6080G, Wellcos Corporation).

[z]E-mail: matic@chalmers.se

Electrochemical testing.—2032 coin cells with Cu foil (Goodfellow, 13 mm diameter) as the working electrode and K metal foil (10 mm diameter) as the counter electrode, separated by a Whatman glass fiber separator sandwiched between two Celgard 2400 separators soaked with 80 μl of electrolyte was used for two-electrode cell tests. The cells were cycled with a Scribner Associates 580 Battery Test System.

Three-electrode cell tests were performed in a custom-built Swagelok–type T cell with a PEEK body and stainless-steel plungers. The working electrode, Cu foil (Goodfellow, 10 mm diameter), and the counter electrode, K metal foil (8 mm diameter), were separated by a separator stack containing a Whatman glass fiber separator sandwiched between two Celgard 2400 separators. The reference electrode was a K metal foil (5 mm diameter), that had been precycled with a slow plating and stripping cycle, 25 μA cm^{-2} for 10 h, following the protocol proposed by Hosaka et al.[24] The reference electrode was separated from the other electrodes with a single Whatman separator. The total electrolyte volume was 80 μl. Electrochemical tests were performed using a VMP3 Multichannel Potentiostat (Biologic).

All cells were assembled in an argon-filled glovebox with oxygen levels below 1 ppm and less than 0.01 ppm H_2O, three-electrode cell tests were performed inside the glovebox and coin cell tests at ambient condition. Precycling to form the SEI layer was done either through a potentiostatic hold at 50 mV vs a K reference/counter electrode (for 15 min unless otherwise noted) or through galvanostatic cycling between 1 and 0.01 V for 5 cycles at 50 μA cm^{-2}, described by Liu et al.[25]

Results and Discussion

At the start of galvanostatic deposition on an inert substrate, such as Cu, the voltage profile typically exhibits a peak (Fig. 1a), commonly associated to the energy barrier for nucleation when ions from the electrolyte are reduced, adsorbed on the substrate,[26] and then need to nucleate to form the bulk metal phase.[27–29] The total energy change during nucleation, ΔG_{Nuc}, is a result of the competition between the surface energy cost of forming a new phase, ΔG_{Surf}, and the energy gain by forming a bulk metal phase on the electrode, ΔG_{Bulk}. For a cap-shaped nucleus, this can be expressed as[29]

$$\Delta G_{\text{Nuc}} = \left(-\frac{4}{3}\pi r^3 \Delta G_V + 4\pi r^2 \gamma \right) f(\theta),$$

where r is the radius of the nucleus, ΔG_V is the Gibbs free energy of supersaturation, γ, is the surface energy between nucleus and electrolyte, and $f(\theta) = \left(\frac{2 - 3\cos\theta + \cos^3\theta}{4} \right)$ is a function of the contact angle, θ, between nucleus and substrate. This equation is plotted for a fixed contact angle in Fig. 1b. Due to the surface energy cost of forming a nucleus, the nuclei need to reach a critical radius, r^*, before they can grow spontaneously, overcoming the energy barrier, $\Delta G_{\text{Nuc}}{}^*$, for the nucleation event.

The energy barrier associated with nucleation will affect the reaction kinetics of the plating as well as the initial morphology through the critical nucleus size.[30,31] If deposition is the only process that takes place, the rate at which atoms are deposited is fixed in a galvanostatic experiment, and the energy barrier, $\Delta G_{Nuc}{}^*$, will be manifested through a larger driving force necessary to drive the reaction at the desired rate. For electrochemical reactions, the thermodynamic driving force is the overpotential,[32] and therefore it is common to observe a larger overpotential at the start of a galvanostatic electrodeposition on a foreign substrate (Fig. 1a).[10,33] Once nucleation has occurred, the deposition mode transitions to growth of deposited structures on the substrate, which has a lower energy barrier and therefore needs a lower driving force to occur at the same rate. Consequently, a peak can be expected, and is often observed, in the voltage profile at the start of galvanostatic deposition. The height of this peak, or nucleation overpotential as defined in Fig. 1a, is frequently used to measure the energy barrier for nucleation.[20] It has also been correlated to the size of deposited nuclei[30] or the interaction between the deposited metal and the substrate.[20]

In practice, the situation is not always this idealized and the other reactions, e.g. SEI formation, need to be accounted for. The influence of side reactions can be observed by comparing deposition on a fresh substrate with the deposition on a substrate where an SEI has been electrochemically formed before the deposition started. To study this, potassium is deposited on Cu electrodes in a highly concentrated KFSI/DME (1:2.5 molar ratio) electrolyte. Electrolytes with different ratios of KFSI and DME have demonstrated potassium stripping and plating with high columbic efficiencies and high salt concentrations also show excellent performance in potassium sulfur full cells.[34,35] Figure 2a shows voltage profiles for galvanostatic deposition of potassium in a two-electrode cell on a fresh Cu surface, on a Cu surface where a potentiostatic hold at 50 mV vs K/K$^+$ has been applied for 15 min prior to the deposition and a Cu surface where an SEI has been formed through a galvanostatic precycling procedure used by Liu et al.[25] (galvanostatic cycling between 1 and 0.01 V for 5 cycles at 50 μA cm^{-2}). Comparing the voltage profiles, we observe a broad and shallow peak at the onset of galvanostatic deposition on the pristine Cu, whereas a deeper and sharper peak appears when a SEI layer is electrochemically formed before the deposition starts (see Fig. 2a). If the size of the thermodynamic barrier for nucleation alone would dictate the height of the overpotential peak, this is an unexpected change. To separate different contributions to the voltage profile, data from a three-electrode cell, allowing the working electrode (WE) and counter electrode (CE)

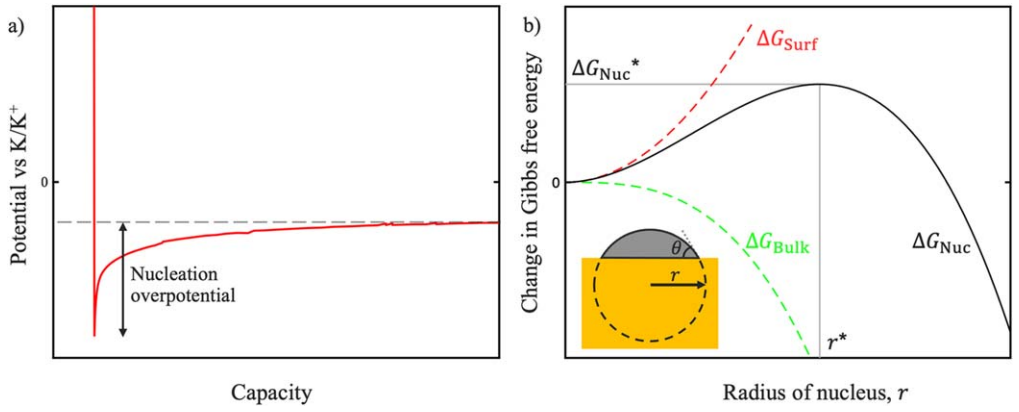

Figure 1. (a) Example of nucleation peak in voltage profile during galvanostatic potassium deposition on Cu. (b) Schematic of Gibbs free energy change of nucleation for a cap shaped nucleus on an inert substrate, together with the individual contributions from surface and bulk energies, see text.

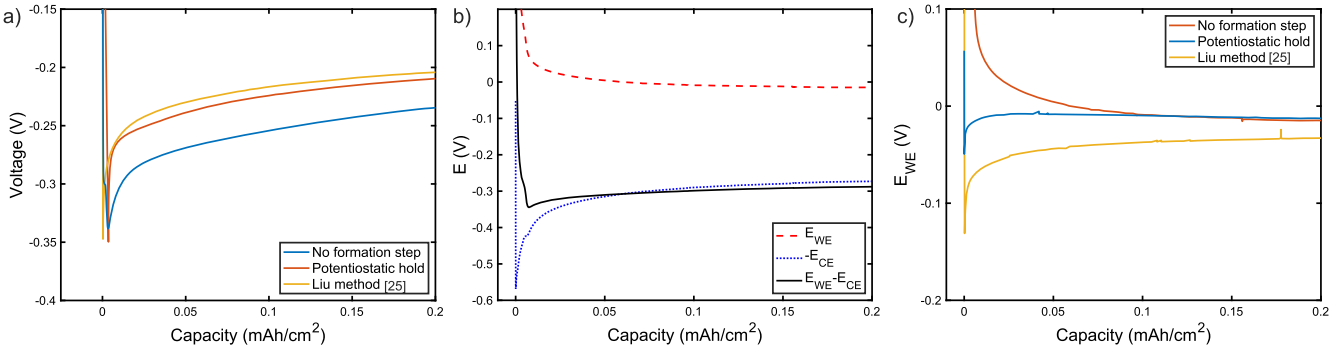

Figure 2. Galvanostatic deposition in K–Cu cells at 0.5 mA cm^{-2}. (a) Voltage profiles from two-electrode coin cells after different SEI formation protocols, see text. (b) Potentials of working (Cu) and counter electrodes (K) in a three-electrode cell where no precycling has been performed. Note that the potential of the counter electrode has been multiplied by −1. (c) Working electrode (Cu) potentials from three-electrode cells where different SEI formation protocols have been applied, see text.

potentials to be tracked individually versus a stable reference, is reported in Fig. 2b where deposition is performed on a fresh Cu surface (i.e. without a SEI formation step). In the three-electrode cell, a peak can be observed in the CE potential while the WE potential shows a smooth decrease. As a result, a peak is observed for the overall cell voltage E_{WE}-E_{CE}, in agreement with the behavior in the two-electrode coin cell. However, this peak is not related to nucleation at the copper surface but instead emanates from the stripping process at the CE. Due to their high chemical reactivity, alkali metal electrodes will always be covered by a surface layer formed through reactions with its ambient atmosphere, even if no electrochemical process has taken place yet.[15,36] The native layer formed inside a glovebox tends to be very resistive, and therefore a large overpotential is required to strip potassium from underneath the native layer. The stripping process will eventually lead to the exposure of fresh potassium which can be stripped at a lower overpotential. This can be compared to observations made for lithium metal electrodes during plating, where plating underneath the native oxide layer has been associated with a higher resistance compared to plating on freshly deposited lithium structures with a less resistive SEI layer.[12,15]

To disentangle the different processes the effect of SEI formation on the voltage profile of the WE is explored in a three-electrode cell, Fig. 2c. After a potentiostatic hold at 50 mV vs K/K^+, a sharp peak appears at the start of the galvanostatic deposition, in contrast to the behavior on a fresh Cu substrate. Similarly, after the precycling scheme adopted by Liu et al.[25] a sharp peak is also observed at the onset of the first galvanostatic deposition. The structure and composition of the SEI are expected to change with the formation protocol, but both SEI formation protocols used here still produce similar voltage profiles.

To aid the interpretation of the voltage profiles of the WE during galvanostatic deposition, the different reactions that take place at the electrode are decoupled using cyclic voltammetry (CV), see Fig. 3a. In the first cycle, a pronounced minimum appears around 0.1 V vs K/K^+ and below 0 V the deposition of potassium is marked by a rapid increase in the current. In the second scan, the current is significantly lower and the minimum around 0.1 V is absent, suggesting the successful formation of an SEI. The reactions taking place are not limited to reduction of the salt (KFSI) and solvent (DME) of the electrolyte, electrolyte impurities as well as copper oxide on the electrode surface are also expected to be reduced in this potential range,[37–39] and underpotential deposition of potassium could, in principle, occur.[40] To better understand the origin of the minimum at 0.1 V, CV scans with varying cutoff potentials are performed consecutively on the same Cu electrode. That is, the potential of the Cu electrode is linearly swept between 2 V and a cutoff potential, which is gradually decreased from 1.0 V to −0.1 V (Fig. 3b). In the final cycle, where the cutoff potential is −0.1 V, a peak appears at 0.16 V in the cathodic scan. This is a signature of stripping from the Cu electrode. Since no peak is observed in any of the previous scans during the cathodic scan, the process occurring around 0.1 V as well as processes occurring at higher potentials in the anodic scan are irreversible and can be ascribed to side reactions and part of the SEI formation. Thus, in this system, competing reactions occur at potentials quite close to those required to deposit potassium metal but no contribution from underpotential deposition is found.

Without a precycling step prior to galvanostatic deposition, side reactions (SEI formation) and potassium deposition can occur simultaneously until the SEI layer has passivated the electrode surface preventing further electrolyte deposition. In this situation, the fixed current can be sustained by SEI formation and nucleation does not need to happen at the particular rate corresponding to the applied current, with the result that a peak does not necessarily appear in the voltage profile. An energy barrier for nucleation still exists, but as nuclei can form at a slower, and perhaps changing rate, no peak in the overpotential is observed. If instead, an SEI formation step is performed before the galvanostatic step, a peak appears since the deposition of potassium is the dominating process. To clarify this argument, a schematic Evans plot is shown in Fig. 3c. This plot shows the relation between the electrode potential and the resulting current for two reactions with different equilibrium potentials, i.e. SEI formation and potassium deposition, as well as the net current produced when the processes take place simultaneously. In this plot, the polarization curves are calculated using the Butler-Volmer equation with an arbitrary set of reaction parameters (charge transfer coefficients 0.5 and identical exchange current densities), making this plot useful only for a qualitative discussion. If the SEI is preformed, then the deposition process needs to produce the entire current set in the galvanostatic experiment i_{set}, which requires an overpotential, E_K. On the other hand, if both the SEI formation and deposition contribute to the net current, a lower electrode polarization, E_{Side+K}, will suffice to produce the same net current. In this case, the deposition (nucleation) can occur at a lower rate. This schematic is of course a simplification of what happens in a real cell, as it does not take into account the self-passivation of the SEI layer, only accounts for a single side reaction and also arbitrarily uses the same exchange current density for the side reaction and for deposition. Still, it clearly illustrates that the presence and height of a nucleation peak does not directly reflect the nature of the nucleation process. The height of the peak can only serve as a measure of the energy barrier for nucleation if other electrochemical processes can be neglected.

If the competition between side reactions and deposition is considered, several observations on the nucleation peak found in literature, as well as the data in Fig. 2, can be explained. Oyakhire et al.[41] previously found that the nucleation peak for the first deposition of Li on Cu became deeper the closer to 0 V vs Li/Li^+ the potentiostatic SEI formation was performed prior to the galvanostatic deposition. The

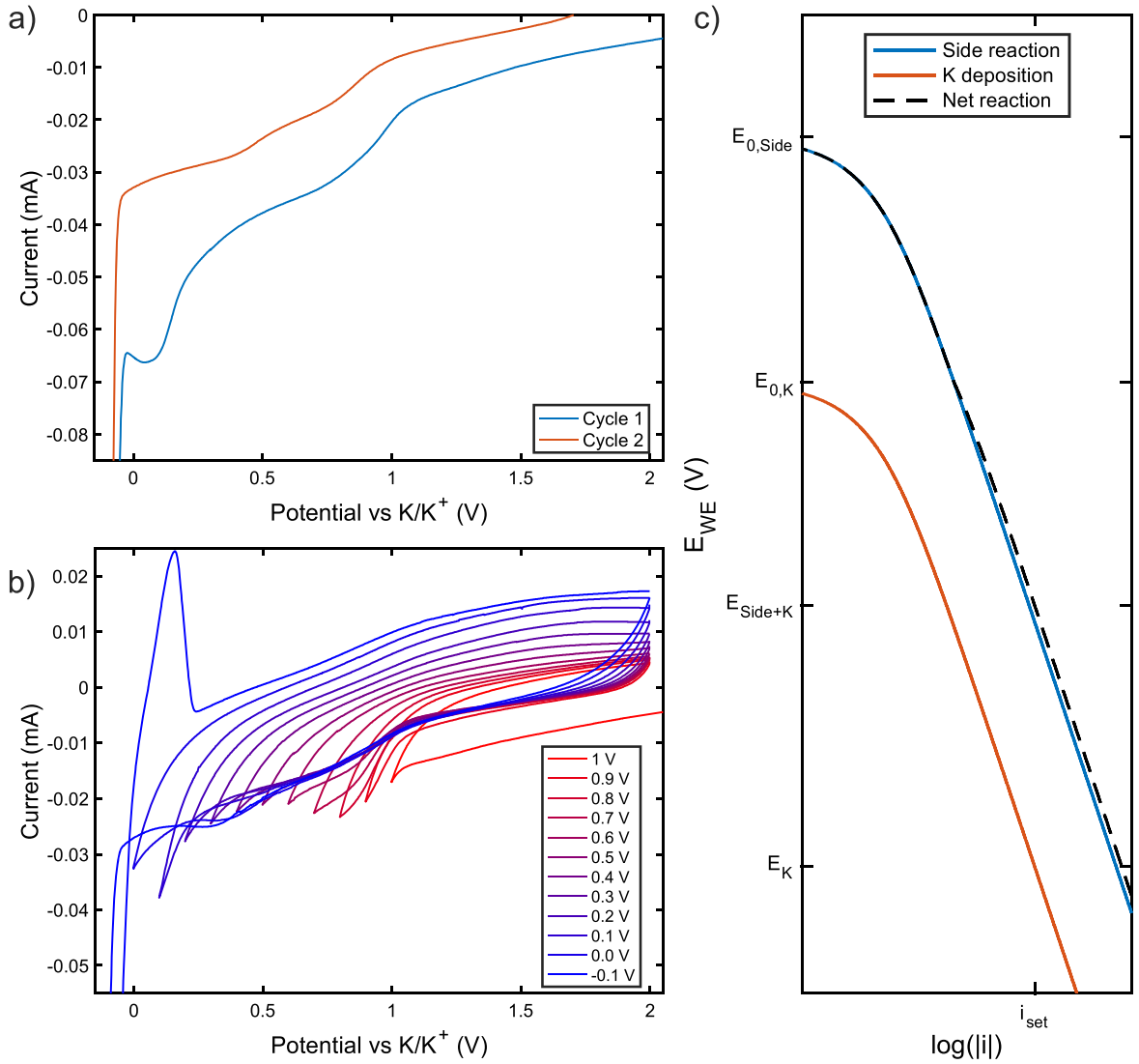

Figure 3. Side reactions and potassium deposition. (a) Anodic scans from the first and second cycle of a CV on copper surface in a three-electrode cell. (b) CV scans on a copper surface in a three-electrode cell with a gradually lowered cutoff potential (see legend). CVs in (a) and (b) are both performed at a scan rate of 1 mV s^{-1}. (c) Evans diagram, illustrating that when a side reaction and potassium deposition occur simultaneously, the expected overpotential is lower.

authors interpreted this as a change in the nucleation barrier, however, it could equally well be explained by the elimination of competing processes prior to the start of the Li deposition. After a potentiostatic hold closer to 0 V vs Li/Li^+ a lower rate of side reactions is expected, consequently nucleation needs to occur at a higher rate, which requires a higher overpotential. Additionally, it has been reported that the alkali metal nucleation peak evolves from the first plating on a substrate to subsequent cycles.[5,42] For a K–Cu cell where galvanostatic stripping/plating is performed on a pristine Cu surface, a smaller overpotential is observed in the first cycle compared to subsequent ones (Fig. S1). This could also be explained by the fact that, without a pre-treatment step, nucleation occurs in parallel with other processes in the first cycle. In subsequent cycles we can expect that the SEI has self-passivated the electrode, Cu_2O on the surface is already reduced and electrolyte impurities have been consumed.

The influence of side reactions on the nucleation peak is also highly dependent on the applied current. Figure S2 shows galvanostatic deposition on Cu surfaces at a lower current, 0.1 mA cm^{-2}, after a potentiostatic hold at 50 mV vs K/K^+ has been applied following the same protocol as for the data in Fig. 2. After a 15 min potentiostatic hold no nucleation peak is observed, pointing to that self-passivation of the electrode has not been fully reached. However, if the hold is prolonged to 5 h, a sharp nucleation peak can be observed (Fig. S2a) and a more well passivating SEI has formed. This can be understood by considering how the current produced during the potentiostatic hold decays over time (Fig. S2b). After a 15 min potentiostatic hold, the current produced by side reactions/SEI formation at 50 mV vs K/K^+ is quite close to 0.1 mA cm^{-2}. Thus, in a subsequent galvanostatic experiment at a low current density this will lead to a situation where the current is dominated by side reactions. On the other hand, after a 5 h hold, the current density corresponding to side reactions is more than one order of magnitude lower than the applied current density. In this situation the behavior at the start of a galvanostatic experiment will be dominated by the nucleation and a nucleation peak appears in the voltage profile (Fig. S2a). Thus, depending on the precycling protocol and the applied current density, differences in the nucleation peak can be observed. Observations in literature also indicate that at high applied current densities the sequence of SEI formation and deposition can change at the onset of galvanostatic cycling. For instance it has been reported that the nucleation peak minimum in Li-Cu cells is reached at larger capacities if a smaller current is applied, indicating that more SEI formation will occur before nucleation starts when a lower current is applied.[33,43] It was also recently proposed that nucleation can outpace SEI formation at extremely high current densities, effectively making the nucleus

shape independent of the SEI.[44] Thus, to observe a nucleation peak where the height correlates with the energy barrier for nucleation, it is central that the applied current density in the experiment is significantly higher than the limiting current in the end of the formation step in order to ensure that nucleation is the dominating process.[41]

After the nucleation step, the galvanostatic cycling will continue with growth as deposition continues followed by stripping when the direction of the current is reversed. In Fig. 4a, the evolution of the voltage profile during subsequent plating–stripping cycles in a K–Cu two-electrode cell is shown. In the first cycle, a large overpotential, around 150–180 mV, can be observed during plating on the WE. The overpotential when potassium is stripped from the WE and plated back on the potassium CE is significantly lower, around 60–70 mV. In the subsequent cycles, a steplike increase in the overpotential is observed during plating on the WE. The second cycle starts at a lower overpotential (60–80 mV), but transitions to a higher overpotential, close to 180 mV, a behavior that has previously also been reported for lithium metal electrodes.[12,15] The initial lower overvoltage plateau was attributed to the stripping of freshly deposited metal from the CE and the higher overvoltage associated with stripping from the bulk CE, covered by surface layers with different interfacial resistances. This scenario is consistent with the appearance of the two-step plateau only in the second cycle in our data, which is the first time during the cycling that there is freshly deposited potassium, without a native oxide layer, on the CE which can be stripped. The contributions from the working and counter electrodes to the total overpotential during cycling are decoupled by three-electrode cell experiments, Fig. 4b, where it is clear that the step in the voltage profile, observed in the second cycle, is indeed arising from the stripping of potassium from the CE. The WE instead shows a low and rather constant overpotential. This step-like voltage profile persists during continued cycling (S3) and analogous features are also observed in K-K coin cells (Fig. S4), only in this case it appears already in the first cycle (the first time there is both fresh and bulk potassium at any of the two electrodes). This changing overpotential during potassium metal stripping from the CE highlights the importance of three-electrode measurements for accurate voltage profile interpretation(s),[45,46] particularly for the evaluation of cathode materials in half-cells where features in the voltage profile emanating from stripping of alkali metal can be erroneously attributed to the processes originating from the active material in the cathode.

To affirm that the step in the voltage profile arises due to the native layer on the potassium metal foil, a potassium electrode is instead prepared by depositing potassium metal directly on a stainless-steel plunger of the three-electrode cell (Figs. S5a–S5b). The cell can then be rebuilt to use this electrochemically formed potassium electrode as the counter electrode in a K–Cu cell (Fig. S5c). This type of potassium electrode does not give rise to the step-like feature (Figs. 4c, S6–8). Other methods to prepare potassium metal electrodes with a reproducible and stable open

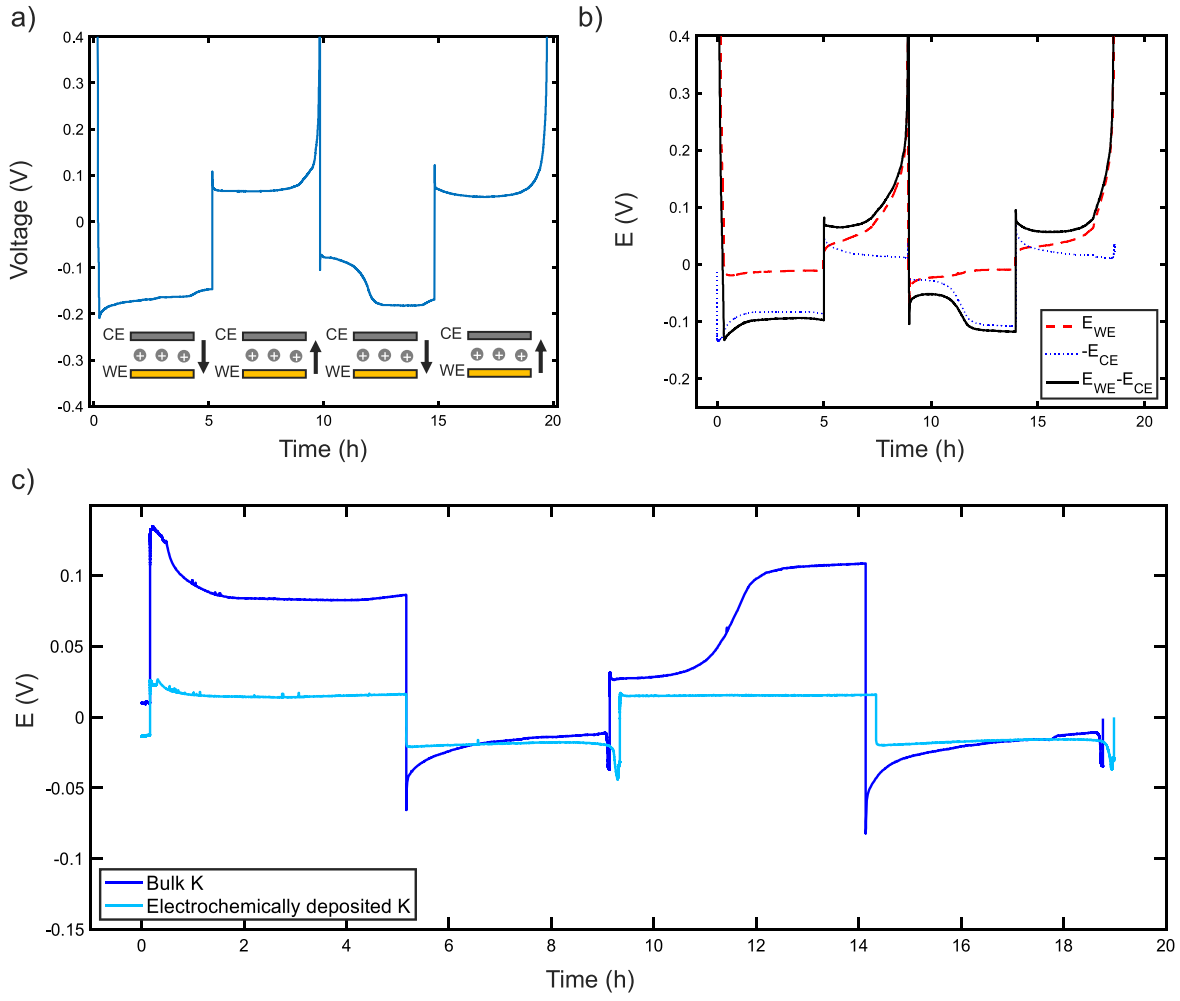

Figure 4. Galvanostatic cycling in K–Cu cells at 0.1 mA cm^{-2}. (a) Evolution of the voltage profile over two plating/stripping cycles in a coin cell (two-electrode) configuration. (b) Contributions to the voltage profile in a three-electrode cell over two plating/stripping cycles. Note that the potential of the counter electrode has been multiplied by −1. (c) Comparison between voltage profiles during galvanostatic cycling for a bulk potassium metal electrode and a potassium electrode which has been formed by electrochemical deposition of potassium metal on a current collector (three-electrode cell).

circuit potential have recently been reported,[24,47] but here a stable stripping/plating potential is also demonstrated. Consequently, the electrochemical preparation of a metal electrode could offer a route to obtain a more stable reference also in two-electrode half-cell configurations.

Conclusions

To summarize, the central processes for the alkali metal anodes discussed in this work, side reactions, nucleation, growth and stripping, often occur in parallel in experiments on symmetric or asymmetric cells. We show a route to disentangle the different processes at each electrode, how they contribute to the voltage profile, and how their interaction and competition between them influence the voltage profile. With this method we demonstrate that the nucleation peak, which is commonly used as a measure of the thermodynamic energy barrier for nucleation on a certain substrate, is very sensitive to the influence of side reactions, such as SEI formation. As shown by our examples, this peak can even be completely absent unless side reactions are separated from the deposition by applying a potentiostatic hold, or using a precycling protocol. Depending on the applied current density, the electrode needs to be passivated to different extents to get a behavior dominated by nucleation in a galvanostatic experiment. This implies that the height of the nucleation peak should not be used as a measure for the energy barrier for nucleation unless sufficient elimination of side reactions can be ensured. In the subsequent processes of deposition and stripping, a steplike voltage profile is often observed from the second cycle and onward in asymmetric coin cells, e.g. K–Cu. This is a result of different resistances for stripping freshly deposited or bulk alkali metal. As potassium is highly reactive, a resistive layer tends to form on foils before they can be placed inside a cell, increasing the overpotential for stripping bulk potassium, whereas the resistivity of the SEI formed on fresh potassium inside the cell is much lower. This results in a voltage profile with two plateaus, indicating that the freshly deposited structures are stripped first, at a lower overpotential, and then the bulk metal is stripped through the more resistive native layer. Clearly, the native surface state of alkali metal electrodes needs to be well controlled to avoid preferential stripping from certain parts of the anode. Further, we emphasize that the voltage profile features of plating and stripping during galvanostatic cycling warrant caution regarding the interpretation of two-electrode half-cell data, for studying nucleation processes as well as evaluating cathode materials or substrate materials for anode-free cells. In this case electrochemically deposited alkali metal on a current collector can be used as a CE to minimize the features in the voltage profile related to the metal electrode.

Acknowledgments

FORMAS and VINNOVA competence center BASE are acknowledged for funding the research.

ORCID

Josef Rizell https://orcid.org/0000-0003-3812-9902
Wojciech Chrobak https://orcid.org/0000-0002-7506-5103
Nataliia Mozhzhukhina https://orcid.org/0000-0001-6798-9704
Shizhao Xiong https://orcid.org/0000-0003-1795-7805
Aleksandar Matic https://orcid.org/0000-0003-4414-9504

References

1. H. Liu et al., *EnergyChem*, **1**, 100003 (2019).
2. J. Qian et al., *Adv. Funct. Mater.*, **26**, 7094 (2016).
3. D. Lin, Y. Liu, and Y. Cui, *Nat. Nanotechnol.*, **12**, 194 (2017).
4. Y. Zhong, S. Zhou, Q. He, and A. Pan, *Energy Storage Mater.*, **45**, 48 (2022).
5. W. Liu, P. Liu, and D. Mitlin, *Chem. Soc. Rev.*, **49**, 7284 (2020).
6. X. B. Cheng, R. Zhang, C. Z. Zhao, and Q. Zhang, *Chem. Rev.*, **117**, 10403 (2017).
7. E. Peled, *J. Electrochem. Soc.*, **126**, 2047 (1979).
8. E. Budevski, G. Staikov, and W. J. Lorenz, *Electrochim. Acta*, **45**, 2559 (2000).
9. W. Plieth, *Electrochemistry for Materials Science* (Elsevier, Amsterdam) 1st ed. (2008).
10. P. Biswal et al., *Proc. Natl. Acad. Sci. U. S. A.*, **118**, e2012071118 (2021).
11. F. Shi et al., *Proc. Natl. Acad. Sci. U. S. A.*, **115**, 8529 (2018).
12. K. N. Wood et al., *ACS Cent. Sci.*, **2**, 790 (2016).
13. K. N. Wood, M. Noked, and N. P. Dasgupta, *ACS Energy Lett.*, **2**, 664 (2017).
14. K. H. Chen et al., *J. Mater. Chem. A. Mater.*, **5**, 11671 (2017).
15. G. Bieker, M. Winter, and P. Bieker, *Phys. Chem. Chem. Phys.*, **17**, 8670 (2015).
16. B. D. Adams, J. Zheng, X. Ren, W. Xu, and J. G. Zhang, *Adv. Energy Mater.*, **8**, 1702097 (2018).
17. J. Xiao et al., *Nat. Energy*, **5**, 561 (2020).
18. C. J. Huang et al., *Nat. Commun.*, **12**, 1452 (2021).
19. B. Wu, J. Lochala, T. Taverne, and J. Xiao, *Nano Energy*, **40**, 34 (2017).
20. K. Yan et al., *Nat. Energy*, **1**, 16010 (2016).
21. B. Lee, E. Paek, D. Mitlin, and S. W. Lee, *Chem. Rev.*, **119**, 5416 (2019).
22. P. Liu and D. Mitlin, *Acc. Chem. Res.*, **53**, 1161 (2020).
23. C. Wei et al., *Energy Storage Mater.*, **30**, 206 (2020).
24. T. Hosaka, S. Muratsubaki, K. Kubota, H. Onuma, and S. Komaba, *J. Phys. Chem. Lett.*, **10**, 3296 (2019).
25. P. Liu et al., *Adv. Mater.*, **34**, 2105855 (2022).
26. L. Chen et al., *J. Power Sources*, **300**, 376 (2015).
27. R. Winand, *Hydrometallurgy*, **29**, 567 (1992).
28. H. Sano, H. Sakaebe, H. Senoh, and H. Matsumoto, *J. Electrochem. Soc.*, **161**, A1236 (2014).
29. Y. Liu et al., *Energy Storage Mater.*, **19**, 24 (2019).
30. Y. Liu et al., *Adv. Sci.*, **8**, 2003301 (2021).
31. M. Z. Bazant, *Acc. Chem. Res.*, **46**, 1144 (2013).
32. E. M. Stuve, *Encyclopedia of Applied Electrochemistry*, ed. G. Kreysa (Springer, New York)p. 1445 (2014).
33. P. Biswal, S. Stalin, A. Kludze, S. Choudhury, and L. A. Archer, *Nano Lett.*, **19**, 8191 (2019).
34. N. Xiao, W. D. Mcculloch, and Y. Wu, *J. Am. Chem. Soc.*, **139**, 94752020 (2017).
35. S. Lee et al., *Adv. Funct. Mater.*, **32**, 2209145 (2022).
36. Y. Li et al., *Nano Lett.*, **17**, 5171 (2017).
37. P. Novak, *Electrochim. Acta*, **30**, 1687 (1985).
38. D. Rehnlund et al., *Nanoscale*, **7**, 13591 (2015).
39. K. Cao et al., *Small*, **15**, 1901775 (2019).
40. D. Aurbach, M. Daroux, P. Faguy, and E. Yeager, *J. Electroanal. Chem.*, **297**, 225 (1991).
41. S. T. Oyakhire et al., *ACS Energy Lett.*, **8**, 869 (2023).
42. A. Mohammadi, L. Monconduit, L. Stievano, and R. Younesi, *J. Electrochem. Soc.*, **169**, 070509 (2022).
43. A. Pei, G. Zheng, F. Shi, Y. Li, and Y. Cui, *Nano Lett.*, **17**, 1132 (2017).
44. X. Yuan, B. Liu, M. Mecklenburg, and Y. Li, *Nature*, **620**, 86 (2023).
45. R. Dugas, J. D. Forero-Saboya, and A. Ponrouch, *Chem. Mater.*, **31**, 8613 (2019).
46. E. C. Cengiz, J. Rizell, M. Sadd, A. Matic, and N. Mozhzhukhina, *J. Electrochem. Soc.*, **168**, 120539 (2021).
47. S. Dhir, B. Jagger, A. Maguire, and M. Pasta, *Nat. Commun.*, **14**, 3833 (2023).